Mid-infrared digital holography and holographic interferometry with a tunable quantum cascade laser

M. Ravaro,[1,2,*] M. Locatelli,[1] E. Pugliese,[1] I. Di Leo,[1] M. Siciliani de Cumis,[1,2] F. D'Amato,[1] P. Poggi,[1] L. Consolino,[1,2] R. Meucci,[1] P. Ferraro,[3] and P. De Natale[1,2]

[1]*INO, Istituto Nazionale di Ottica—CNR, Largo E. Fermi 6, Firenze I-50125, Italy*

[2]*LENS, European Laboratory for NonLinear Spectroscopy, Via N. Carrara 1, Sesto Fiorentino (FI) I-50019, Italy*

[3]*INO, Istituto Nazionale di Ottica—CNR—Sezione di Napoli, Via Campi Flegrei, 34 80078 Pozzuoli (Napoli), Italy*

**Corresponding author: marco.ravaro@ino.it*

Received June 12, 2014; accepted June 26, 2014;
posted July 11, 2014 (Doc. ID 213934); published August 13, 2014

Mid-infrared digital holography based on CO_2 lasers has proven to be a powerful coherent imaging technique due to reduced sensitivity to mechanical vibrations, increased field of view, high optical power, and possible vision through scattering media, e.g., smoke. Here we demonstrate a similar and more compact holographic system based on an external cavity quantum cascade laser emitting at 8 μm. Such a setup, which includes a highly sensitive microbolometric camera, allows the acquisition of speckle holograms of scattering objects, which can be processed in real time. In addition, by exploiting the broad laser tunability, we can acquire holograms at different wavelengths, from which we extract phase images not subjected to phase wrapping, at synthetic wavelengths ranging from hundreds of micrometers to several millimeters.

OCIS codes: (090.1995) Digital holography; (090.2880) Holographic interferometry; (140.5965) Semiconductor lasers, quantum cascade.

http://dx.doi.org/10.1364/OL.39.004843

Extension of hologram recording to the infrared (IR) spectrum has attracted considerable interest since the early stages of holography [1], due to the relaxation of the mechanical stability requirements and to the IR transparency of various materials opaque to visible radiation. In addition, IR hologram recording intrinsically benefits from a larger field of view and is well suited for measuring optical path variations, reducing the recourse to phase unwrapping algorithms [2]. On the other hand, whereas powerful and highly coherent CO_2 lasers have quickly established themselves as convenient light sources for this purpose, the search for a suitable IR recording medium has turned out to be challenging [3]. Recording media reported were not satisfactory in terms of either IR recording sensitivity or maximum resolution. Only in the last decade, in the wake of establishment of digital holography in the visible range, with CCD and CMOS sensors replacing photographic plates [4,5], IR holography has finally acquired momentum, which is due to the recent development of pyrocameras and focal plane array microbolometers [6,7]. Thanks to sensors, composed of hundreds of thousands of pixels as small as a few tens of micrometers and operating at room temperature, CO_2 laser-based IR holography has proven its potential for applications. Mid-IR digital holography is now an appealing tool for, e.g., on-site industrial nondestructive testing or, after demonstration of vision capability through smoke and flames, for rescuing people during fires [8,9].

Quantum cascade laser (QCL) operation was demonstrated in 1994, and QCLs have, since then, achieved dramatic performance improvement thus becoming, nowadays, the semiconductor source of choice in the mid-IR, featuring output power up to the Watt level, single-mode operation, and a broad tuning range [10]. Although QCLs feature a lower output power compared with that of CO_2 lasers, they appear as attractive sources for mid-IR holography, due to their compactness and to the coverage of different regions of the mid-IR spectrum, ranging from 3 to 16 μm. Moreover, the present availability of QCLs oscillating in an external cavity with a broad tuning range makes QLCs attractive sources for holographic interferometry [11]. Phase imaging in digital holography is a straightforward and well-known technique to measure optical path lengths, but possibly requires the use of a phase-unwrapping algorithm to remove 2π discontinuities [12,13]. Multiple wavelength hologram acquisition is an elegant approach to get around such a major drawback by measuring the phase at a synthetic wavelength,

$$\Lambda_{12} = \frac{\lambda_1 \lambda_2}{|\lambda_1 - \lambda_2|}, \tag{1}$$

which is much longer than the actual wavelengths (λ_1, λ_2) of the lasers employed [14]. In particular, the use of a tunable laser rather than a pair of fixed wavelength lasers allows: (1) choosing a synthetic wavelength adjusted to the optical path length to be measured; (2) maintaining the low-noise precision of a short wavelength measurement by hierarchical phase unwrapping based on phase images at multiple synthetic wavelengths [15,16]. In this work, we report the first demonstration of mid-IR digital holography based on a tunable QCL. By means of a high-sensitivity thermographic camera, we could acquire speckle holograms of scattering objects, which could be processed in real time. In addition, by exploiting the large tuning range of the QCL, we could extract phase-images at several synthetic wavelengths, thus largely extending the optical path range of mid-IR holographic interferometry.

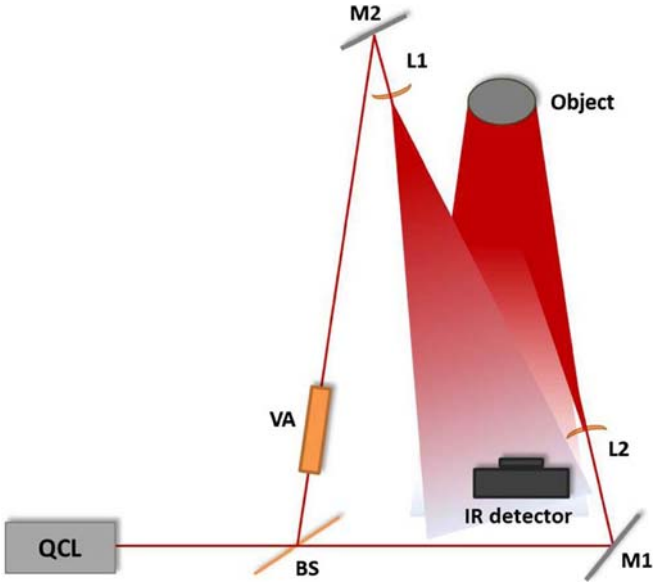

Fig. 1. Experimental setup for mid-IR hologram acquisition. M, metallic mirrors; L1 and L2, ZnSe lenses; VA, ZnSe variable attenuator; BS, ZnSe beam splitter. The angle between object beam and reference beam is ≈8°, the distance object-IR detector ≈25 cm, and the distance L1-IR detector ≈27.5 cm.

The QCL used throughout our experiments, produced by Daylight Solutions, is equipped with a Littrow-mounted motorized grating and can be tuned by ≈0.7 μm around 8 μm. When operated in CW mode, it emits, at room temperature, up to 80 mW in a low-divergence (≤5 mrad) TEM_{00} beam. It was used in combination with a room-temperature thermocamera, produced by Thermoteknix, designed for the 8–12 μm spectral range, with a frame rate of 50 s^{-1}, based on an array of 640 × 480 microbolometers, with a pixel pitch of 25 × 25 μm. The hologram acquisition setup was arranged in a lensless off-axis configuration (Fig. 1): the QCL beam was first divided by a ZnSe beam splitter (BS) into a reflected reference beam (20%) and a transmitted object beam (80%). The former beam was passed through a ZnSe variable attenuator (VA) and an $f = 1$ in. ZnSe lens (L1), which focused it and then enlarged it in order to obtain almost planar wavefront impinging on the thermocamera. The object beam was focused by a $f = 120$ mm ZnSe lens (L2), so as to expand it and entirely illuminate the targeted object. The angle between the reference beam and the scattered object beam impinging on the camera was chosen, so as to obtain a fringe spatial frequency suitable to separate the real image from the virtual one, without violating the Nyquist criterion. The maximum optical path difference between reference and object beams was kept below the QCL beam coherence length:

$$L = \frac{c}{\Delta\nu} \geq 3 \text{ m}, \tag{2}$$

(QCL linewidth $\Delta\nu \leq 100$ MHz). Both beams were vertically polarized as the QCL output beam, since none of the optical elements in the experimental setup can induce a polarization rotation.

IR holograms were acquired by a computer at a frame rate of 25 s^{-1} and monitored in real time. This allowed fine-tuning the reference beam power, so as to maximize the fringe contrast on the camera and improve the quality of the reconstructed image. Figure 2(a) shows the IR hologram of a small bronze statue, about 10 cm high, reproducing emperor Augustus [Fig. 2(c)], acquired at $\lambda_{QCL} = 8$ μm. The maximum object dimension was dictated by the available laser power. Due to the large field of view accessible in this spectral range, a more powerful QCL would enable uniform irradiation and acquisition of holograms of much larger objects, as already demonstrated by using a CO_2 laser [17]. Acquired frames were numerically elaborated by means of a routine based on the Fresnel method, extracting amplitude and phase reconstructed holograms, which could be observed in real time at a frame rate of 5 s^{-1}. The amplitude reconstruction of the hologram in Fig. 2(a) is reported in Fig. 2(b), where the unwanted diffraction orders have been filtered, and a numerical enhancement has been performed to improve the image quality. We stress that table vibration damping was not necessary during acquisition, thanks to the aforementioned intrinsic robustness of the system to mechanical vibrations.

In order to test the capabilities of our acquisition system for holographic interferometry, we acquired a set of holograms of a small aluminum wedge, $h = 29$ mm high, with an angle $\alpha = 20°$ between the two planes [Fig. 3(a)]. The back plane of the wedge was oriented orthogonally

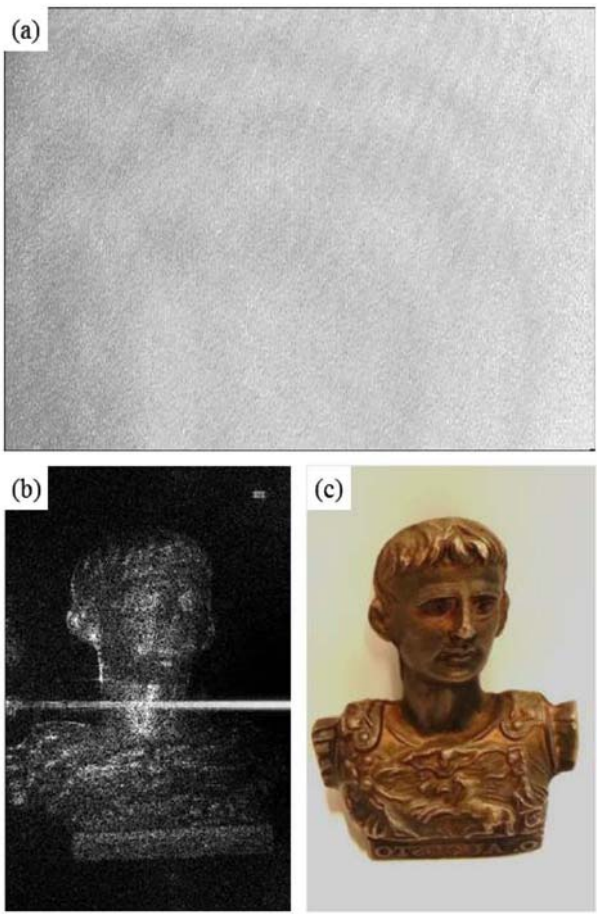

Fig. 2. (a) 640 × 480 pixel 8 μm hologram of Augustus bronze statue. (b) Reconstructed amplitude; only one diffraction order is shown. (c) Picture of the statue.

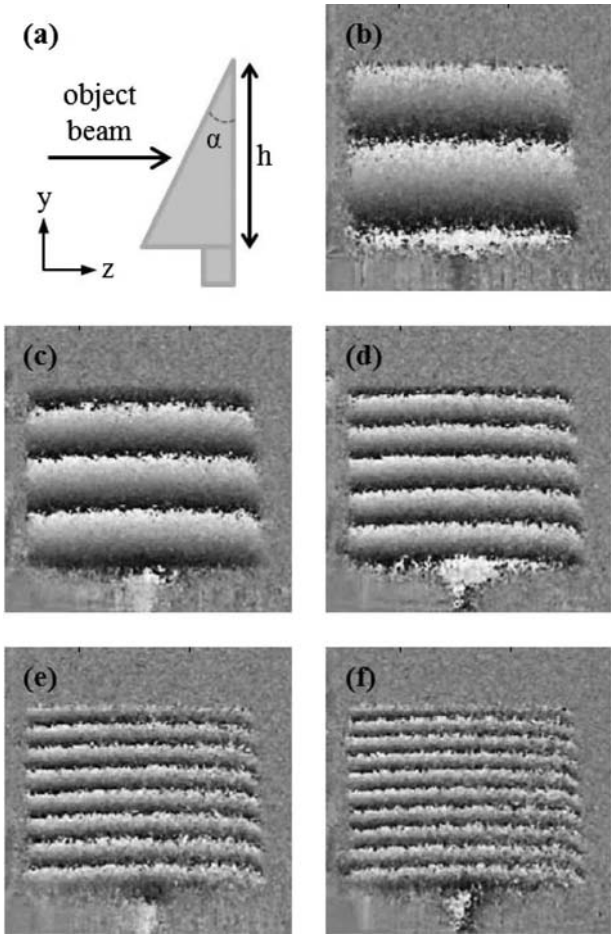

Fig. 3. (a) Sketch of the Al wedge imaged. Phase images of the wedge front plane at synthetic wavelengths (b) $\Lambda_{01} = 9.7$ mm, (c) $\Lambda_{02} = 5.0$ mm, (d) $\Lambda_{04} = 3.4$ mm, (e) $\Lambda_{06} = 2.6$ mm, and (f) $\Lambda_{08} = 2.1$ mm. The wedge was sand blasted with 10 μm particles in order to increase the amount of scattered light.

to the incoming object beam (assumed to have a planar wavefront), so that the impingement angle on the wedge front plane was equal to α. Accordingly, for a given pair of impingement points (x_a, y_a) and (x_b, y_b) on the wedge front plane, the measured optical path difference is $\Delta z_{ab} = 2\Delta y_{ab} \tan(\alpha)$. By computing the difference between the reconstructed phase of holograms acquired at λ_i and λ_j, such path difference results in dephasing:

$$\Delta\varphi_{ij} = 2\pi \frac{|\lambda_i - \lambda_j|}{\lambda_i \lambda_j} \Delta z_{ab} = 2\pi \frac{\Delta z_{ab}}{\Lambda_{ij}}. \quad (3)$$

The full wavelength tuning range of our QCL results in a minimum synthetic wavelength $\Lambda_{ij} \approx 0.1$ mm. Such a range, however, is not spanned continuously, since the cavity length of the laser is not adjusted while the grating is rotated to change the wavelength. As a result, grating tuning occurs through mode hops of 3–10 nm. This implies that the maximum synthetic wavelength Λ_{ij}, which could be extremely large in case of continuous tuning, is in practice limited to ≈20 mm.

IR holograms of the wedge were acquired at nine different wavelengths λ_i with $i = 0, 1, \ldots 8$, ranging from 8 to 7.969 μm. By subtracting the reconstructed phase for λ_0 to those obtained for λ_j with $j = 1, 2, \ldots 8$, we obtained the phase φ_{0j} at the synthetic wavelengths Λ_{0j}, ranging from 9.7 to 2.1 mm. Figure 3(b) shows the φ_{01} phase image of the wedge front plane: the measured phase is constant in the horizontal direction while, in the vertical direction, it varies from the top to the base of the wedge by about 4π, i.e., the maximum optical path difference is approximately equal to twice the synthetic wavelength $\Lambda_{01} = 9.7$ mm. The reconstruction algorithm folds such phase variation in the $0 - 2\pi$ range, thus originating two fringes. Such fringes are not perfectly straight, and their period is not exactly constant due to nonideality of the object and the reference beam wavefront. As shown in Figs. 3(c)–3(f), by reducing the synthetic wavelength, the number of fringes increases, as expected. By inspecting the phase along horizontal lines, we found phase speckle fluctuations of the order of 1 rad, resulting in a noise on the measured optical path difference Δz proportional to the synthetic wavelength and ranging from 1.5 mm (Λ_{01}) to 0.3 mm (Λ_{08}) [12]. Note that, in all the phase images the speckle spike noise was reduced through the use of a median filter, i.e., by replacing each local phase value with the median of its 3×3 pixel neighborhood.

The number n of fringes measured in the different phase images is summarized in Fig. 4 as a function of the equivalent wavelength (in terms of wavenumber). The x error bar of ± 0.25 cm^{-1} is determined by the mode hop tuning of the QCL, since the wavelength λ was not measured but simply inferred from the grating angle. The experimental data points follow a linear trend and are fully consistent with the expected number of fringes $n = 2h \times \tan(\alpha)(1/\Lambda)$, i.e., the straight line in Fig. 4. After validation, multiple wavelength holographic interferometry was exploited to acquire phase images of a coin: Fig. 5(a) shows the reconstructed amplitude at 8 μm, while Figs. 5(b)–5(f) show the phase images at the synthetic wavelengths $\Lambda = 10$, 5, 3.3, 2.5, and 2 mm. By reducing the synthetic wavelength down to a value matching the asperities of the object surface, the phase-noise amplification is reduced, as explained above, while the contrast is visibly improved. In this respect,

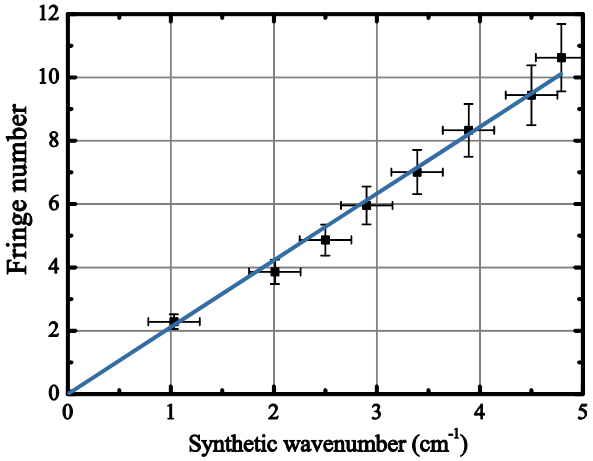

Fig. 4. Number n of fringes imaged on the wedge front plane versus synthetic wavenumber $1/\Lambda$ (squares). The experimental data points, considered the x and y error bars, are compatible with the expected number of fringes $n = \Delta\varphi(\Delta z = h)/2\pi = 2h \times \tan(\alpha)(1/\Lambda)$ (blue solid line).

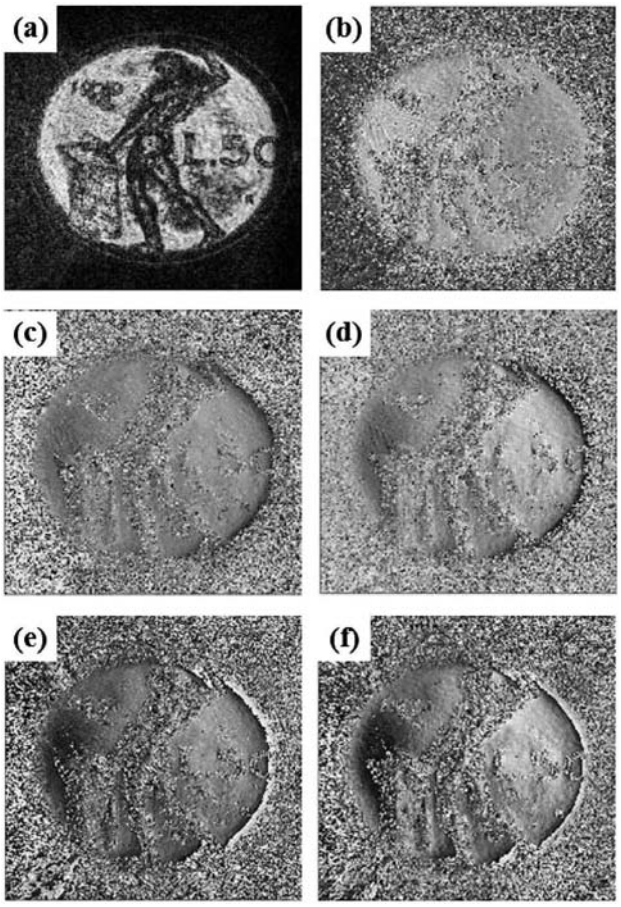

Fig. 5. (a) Amplitude reconstruction. Phase reconstruction at synthetic wavelengths (b) $\Lambda = 10$ mm, (c) $\Lambda = 5$ mm, (d) $\Lambda = 3.3$ mm, (e) $\Lambda = 2.5$ mm, and (f) $\Lambda = 2$ mm of a 50 Lire coin. Also in this case, the object was sand blasted in order to increase the amount of scattered light.

note that in this case the phase images have not been processed with the median filter in order to avoid the consequent resolution loss.

From what was described, it turns out that illumination by means of QCLs is a helpful solution for mid-IR digital holography with respect to the use of widespread but bulky CO_2 lasers. For small object imaging, when the required laser power is not exceeding 1 W, QCLs allow setting up compact and portable acquisition systems. In addition, availability of tunable devices operating in an external cavity makes a QCL especially suitable for holographic interferometry, enabling the measurement of optical path lengths with an adjusted synthetic wavelength, thanks to flexible multiple wavelength hologram acquisition. Hologram acquisition based on a tunable QCL also opens a new approach to the stand-off detection of dangerous materials with high molecular weight, allowing the study of molecular spectra with large (10/50 cm^{-1}) absorption bands in environmental monitoring [18] and for security applications [19,20]. Such techniques can be exploited in the various frequency regions of the mid-IR spectrum covered by QCLs and, in perspective, also in the THz spectrum, which is especially attractive for imaging due to the relatively high transparency of materials such as wood, paper, clothes, and plastics or for improvements in biomedical diagnostic [21].

This work was partly supported by the Italian Ministry of Education, University and Research (MIUR) through the program "FIRB–Futuro in Ricerca 2010" RBFR10LULP.

References

1. J. S. Chivian, R. N. Claytor, and D. D. Eden, Appl. Phys. Lett. **15**, 123 (1969).
2. M. P. Georges, J.-F. Vandenrijt, C. Thizy, Y. Stockman, P. Queeckers, F. Dubois, and D. Doyle, Appl. Opt. **52**, A102 (2013).
3. R. M. Beaulieu and R. A. Lessard, Proc. SPIE **3011**, 298 (1997).
4. U. Schnars and W. Jueptner, Appl. Opt. **33**, 179 (1994).
5. U. Schnars and W. Jueptner, J. Opt. Soc. Am. A **11**, 2011 (1994).
6. E. Allaria, S. Brugioni, S. De Nicola, P. Ferraro, S. Grilli, and R. Meucci, Opt. Commun. **215**, 257 (2003).
7. M. Paturzo, A. Pelagotti, A. Finizio, L. Miccio, M. Locatelli, A. Geltrude, P. Poggi, R. Meucci, and P. Ferraro, Opt. Lett **35**, 2112 (2010).
8. M. Locatelli, E. Pugliese, M. Paturzo, V. Bianco, A. Finizio, A. Pelagotti, P. Poggi, L. Miccio, R. Meucci, and P. Ferraro, Opt. Express **21**, 5379 (2013).
9. J.-F. Vandenrijt, C. Thizy, I. Alexeenko, G. Pedrini, J. Rochet, B. Vollheim, I. Jorge, P. Venegas, I. López, W. Osten, and M. P. Georges, Opt. Eng. **52**, 101903 (2013).
10. J. Faist, *Quantum Cascade Lasers* (Oxford, 2013).
11. R. Maulini, I. Dunayevskiy, A. Lyakh, A. Tsekoun, C. K. N. Patel, L. Diehl, C. Pfluegl, and F. Capasso, Electron. Lett. **45**, 107 (2009).
12. M. Servin, J. L. Marroquin, D. Malacara, and F. J. Cuevas, Appl. Opt. **37**, 1917 (1998).
13. A. Asundi and Z. Wensen, Appl. Opt. **37**, 5416 (1998).
14. L. O. Heflinger and R. F. Wuerker, Appl. Phys. Lett **15**, 28 (1969).
15. A. Wada, M. Kato, and Y. Ishii, Appl. Opt. **47**, 2053 (2008).
16. C. J. Mann, P. R. Bingham, V. C. Paquit, and K. W. Tobin, Opt. Express **16**, 9753 (2008).
17. A. Geltrude, M. Locatelli, P. Poggi, A. Pelagotti, M. Paturzo, P. Ferraro, and R. Meucci, Proc. SPIE **8082**, 80820C (2011).
18. M. Siciliani de Cumis, F. D'Amato, S. Viciani, B. Patrizi, P. Foggi, and C. L. Galea, Laser Phys. **23**, 025603 (2013).
19. F. Fuchs, J. Phillip Jarvis, S. Hugger, M. Kinzer, Q. Yang, W. Bronner, R. Driad, and R. Aidam, Comm. Comp. Info. Sci. **318**, 388 (2012).
20. A. Skvortsov, Quantum Electron. **42**, 1 (2012).
21. A. J. Fitzgerald, V. P. Wallace, M. Jimenez-Linan, L. Bobrow, R. J. Pye, A. D. Purushotham, and D. D. Arnone, Radiology **239**, 533 (2006).